Citation: R. Herguedas, G. Lopez-Nicolas, C. Sagues. Collision-free Transport of 2D Deformable Objects. International Conference on Control, Automation, and Systems (ICCAS 2021), Jeju, Korea, October 12-15, 2021.

2021 The 21st International Conference on Control, Automation and Systems (ICCAS 2021)
Ramada Plaza Hotel, Jeju, Korea, Oct. 12∼15, 2021

Collision-free transport of 2D deformable objects

Rafael Herguedas*, Gonzalo López-Nicolás and Carlos Sagüés

Instituto de Investigación en Ingeniería de Aragón, Universidad de Zaragoza, Zaragoza, Spain
{rherguedas, gonlopez, csagues} @unizar.es * Corresponding author

Abstract: In this paper, we propose a novel system to transport 2D cloth-like deformable objects with mobile manipulators and without collisions along a known path. First, a new deformation model that allows for real-time shape prediction, based on the paradigm of deformable bounding box, is presented. Then, observability index maximization is applied to obtain the model parameters with a reduced number of measurements. The transport task is next defined as an optimization problem that incorporates the computed model and the transport route. A set of linear and nonlinear constraints allows to limit the object's deformations and rotations and to avoid obstacles, respectively. Simulation results are reported to demonstrate the validity of our method.

Keywords: Mobile Manipulation; Collision Avoidance; Multi-Robot Systems

1. INTRODUCTION

Autonomous manipulation and transport of deformable objects is nowadays an active discipline in robotics [1]. This topic seems particularly interesting for industrial and medical applications that deal with objects which are difficult to handle, toxic substances or infected materials. In these cases, limiting human intervention could prevent the workers from being injured or contaminated. In addition, the logistics sector can obtain great benefits from autonomous transport of deformable objects, given the increasing number and the variety of consumer goods. Using a multi-robot team to perform these kinds of tasks allows not only to autonomously transport large size or heavy deformable objects, but it also increases the system efficiency and flexibility [2].

In working environments such as industries, the traffic of people and materials is usually predetermined and highly controlled. In particular, in the textile and footwear sectors, among others, large pieces of fabric are transported between different workstations in which they are progressively transformed. From this perspective, we develop a multi-robot transport system of cloth-like deformable objects that follows a prescribed route across the environment. Due to the fact that obstacles may appear in the given path, the system deforms and/or rotates the transported object as required to avoid collisions, with minimal displacements of the manipulators. Minimal displacements are convenient in order to reduce the object deformation, the energy consumption and the number of maneuvers of the manipulators. The transported object is considered linear elastic, but its mechanical properties are unknown to the system. Deformation and rotation of the object are obtained by means of the *deformable bounding box* (DBB) geometric model (see Fig. 1), which is identified from a reduced set of measurements.

In general, one of the main concerns when dealing with manipulation of deformable objects is to control deformation effectively. Model-based approaches are more common than those not considering deformation models [3], and many of them develop geometric strategies due to their numerous advantages. Focused on spatial constraints, geometric methods are based on assumptions about the object that allow to quickly estimate its shape under different grasping configurations [4].

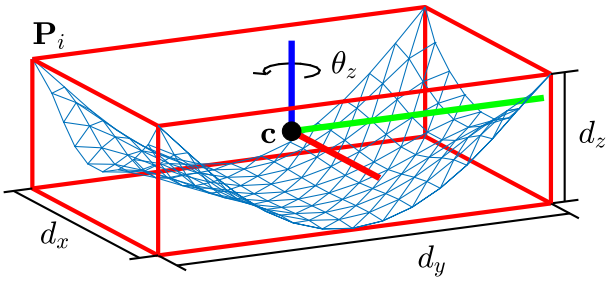

Fig. 1. Bounding box (BB) of an elastic sheet, held by its four corners. Its main parameters are: the BB centroid $\mathbf{c}$, the BB dimensions d_x, d_y and d_z, the BB rotation around the vertical axis θ_z and a grasping point $\mathbf{P}_i$. The bold lines in red, green and blue represent the BB x-y-z reference frame.

Jacobian matrix based approaches provide a convenient relation between deformation and the derivative of the action that originates deformation. They can be adopted in combination with other techniques, as the previously referred geometric methods. Hosoda and Asada developed a visual servoing control strategy in which the Jacobian of the robotic manipulator is estimated without the knowledge of the true kinematic parameters [5]. A different visual servo controller by Navarro-Alarcon *et al.* [6] estimates from visual feedback the deformation Jacobian matrix in real-time. The work by Ruan *et al.* [4] also considers an approximated Jacobian for driving a deformable object to a target shape. The Jacobian is here estimated with a method based on the concept of diminishing rigidity. Recently, a cable manipulation framework has been proposed with real-time estimation of the Jaco-

This work was supported by projects COMMANDIA SOE2/P1/F0638 (Interreg Sudoe Programme, ERDF), PGC2018-098719-B-I00 (MCIU/AEI/FEDER, UE) and DGA_T45-17R (Gobierno de Aragón). The first author was partially supported by the EU through the European Social Fund (ESF) "Construyendo Europa desde Aragón".

bian matrix, which represents a local linear deformation model [7].

The idea of a deformable bounding box has been previously exploited in different ways and for various purposes. Burchan *et al.* [8] described a probabilistic roadmap motion planing strategy for deformable robots where the robot's deformation is obtained from a deformed bounding box. Navigation through confined spaces is the objective pursued by Buchanan *et al.* [9], which they accomplish by appliying the concept of deformable bounding box as an abstraction of an hexapod robot model. In this case, the bounding box has fixed length and height, and width is the variable dimension. Also Tallamraju *et al.* [10] consider a 2D deformable bounding box for motion planning, but their objective is to transport a rigid payload with a team cooperative mobile manipulators. Unlike these studies, we conceive the DBB as a versatile 3D deformation model that accounts for variations in all dimensions of the box (length, height and width), which must be identified for each different combination of objects and manipulator configurations.

Cooperative transport of deformable objects includes early developments [11] and more recent ones [12], [13]. These studies deal with a common goal: performing path planning without collisions with multiple manipulators, which carry different deformable loads. In contrast to our approach, these studies do not consider computing a deformation model of the transported object or minimizing the motions that deform and rotate the object. We also developed a strategy for simultaneous shape control and transport of deformable objects [14]. In this previous work, obstacle avoidance was not specifically addressed.

Our main contributions in the present study are a new 3D deformation model based on the DBB paradigm and the proposal of the optimization problem that allows navigation without collisions with minimal relative movements of the grippers.

2. PROBLEM STATEMENT

Let us consider a large 2D cloth-like linear elastic object being carried in a 3D environment by a set of $N \geq 3$ robots, each one equipped with a fixed gripper. The robots obey single-integrator kinematics and they grasp a set of points $\mathbf{P} = \{\mathbf{P}_i = [P_{ix}, P_{iy}, P_{iz}]^T, i = 1, ..., N\}$ of the object's boundary. These robot-object links are modeled as spherical joints. The sequence of target points over time $\mathbf{r} = \{\mathbf{r}_k = [r_{xk}, r_{yk}]^T, k = 1, ..., \mathrm{T}\}$ prescribes the route in the plane the object's centroid must follow. This path passes through obstacles, which are detected by the robots with onboard range sensors. A perception range R is set for the robotic system, and the M obstacle points lying within this range are aggregated in a global point cloud $\mathbf{Q} = \{\mathbf{Q}_j = [Q_{jx}, Q_{jy}, Q_{jz}]^T, j = 1, ..., M\}$. The shape of the object is represented by its *bounding box* (BB), defined by the centroid $\mathbf{c} = [c_x, c_y, c_z]^T$, which is expressed in the global reference frame, the dimensions $\mathbf{d} = [d_x, d_y, d_z]^T$ and the rotation θ_z, which are expressed in the BB reference frame (see Fig. 1).

The absolute velocity of the grasping point $\mathbf{P}_i$ in the global reference is computed as

$$\dot{\mathbf{P}}_i = \dot{\mathbf{P}}_t + \dot{\mathbf{P}}_{di} \ . \tag{1}$$

$\dot{\mathbf{P}}_t$ is the transport velocity of the grippers, that produces global translation of the object along the target points $\mathbf{r}$, and is given *a priori* by the task definition. The velocity of the grasping point with respect to the object $\dot{\mathbf{P}}_{di}$ applies the actions that are responsible for obstacle avoidance to the object. These actions, which we assume quasi-static and are expressed in the BB reference frame, are traction/compression deformations in the horizontal plane $\mathbf{G} = [G_x, G_y, 0]^T$ and rotation around the vertical axis ϕ_z. Note that in case no deformation is applied to the BB, $\theta_z = \phi_z$.

Our system is conceived to transport an object so that its centroid follows the given path without collisions, by effectively exploiting the deformation properties of the transported object. We seek to minimize the velocities of the manipulators with respect to the object $\dot{\mathbf{P}}_{di}$. Thus, we define the following cost function:

$$\gamma = \sum_{i=1}^{N} \|\dot{\mathbf{P}}_{di}\| \ . \tag{2}$$

Minimizing this cost function is appropriate not only to reduce the object deformation and the energy consumption of the robots, but also for safely driving the system with minimal motions.

3. DEFORMABLE BOUNDING BOX MODEL

3.1 Model overview

In this section, we present a novel deformation model based on the paradigm of *deformable bounding box*.

Definition 1: **Ground-parallel bounding box.** The ground-parallel bounding box (GPBB) is the minimal box that contains the object at certain instant and whose top and bottom faces are parallel to the ground plane.

The GPBB is the ground-parallel box that best approximates the real shape of the object. Then, the variation over time of the dimensions and rotation of the object's GPBB, $\dot{\mathbf{d}} = [\dot{d}_x, \dot{d}_y, \dot{d}_z]^T$ and $\dot{\theta}_z$, is what we model with the DBB. While this model is unable to explain local effects and limits the kinds of actions that can be applied to the object, it also presents different advantages. Its compact and general structure allows to encapsulate the properties of objects with different shapes and sizes, grasped with different number of grippers in diverse configurations. The model can be rapidly determined for each system due to its reduced number of parameters, and when using it for optimization, as we will describe in Section 4, it can be efficiently evaluated.

Our target problem requires to modify the shape of the object over time in order to avoid obstacles. Therefore,

the dimensions of the object's BB are going to change over time too. The DBB model we propose can be expressed in a Jacobian matrix that maps the inputs of the grippers to the dimensional and rotational derivatives of the BB:

$$\left[\dot{d}_x \;\; \dot{d}_y \;\; \dot{d}_z \;\; \dot{\theta}_z\right]^T = \mathbf{J}\,\mathbf{u} = \mathbf{J}\left[\dot{G}_x \;\; \dot{G}_y \;\; \dot{\phi}_z\right]^T , \quad (3)$$

being $\mathbf{J} = [k_{ij}]$ with $i = \{1, ..., 4\}$ and $j = \{1, 2, 3\}$,

$$\dot{\mathbf{d}} = \left(\mathbf{d}_k - \mathbf{d}_{(k-1)}\right) \oslash \left(\mathbf{d}_{(k-1)}\;(t_k - t_{(k-1)})\right) , \quad (4)$$

and similarly for $\dot{\mathbf{G}}$,

$$\dot{\theta}_z = (\theta_{zk} - \theta_{z(k-1)})/(t_k - t_{(k-1)}) , \quad (5)$$

and similarly for $\dot{\phi}_z$, where '$\oslash$' is the element-wise division and $t_k - t_{(k-1)}$ is the time interval between the states $\mathbf{d}_k$ and $\mathbf{d}_{(k-1)}$.

The interaction matrix $\mathbf{J}$ in (3) includes 12 different parameters, 9 of which vary depending on the object properties and the number and configuration of the grippers. We consider that $k_{13} = k_{23} = k_{33} = 0$, provided that the rotation velocity is small and, therefore, deformations are independent from the global rotations of the object, i.e. centrifugal effects are negligible. It can be seen that the deformation velocities $\dot{\mathbf{d}}$ and $\dot{\mathbf{G}}$ are given as a ratio. This is a requirement for having an appropriate scaling of the deformation and rotation units, and it is also common when defining deformations in the framework of solid mechanics. The gripper relative velocities $\dot{\mathbf{P}}_{di}$ can be computed from the inputs $\mathbf{u}$ in the following manner:

$$\dot{\mathbf{P}}_{di} = \mathbf{R}\left([0, 0, \dot{\phi}_z]^T \times \mathbf{p}_i + (\dot{\mathbf{G}} \circ \mathrm{sgn}(\mathbf{p}_i))/2 \circ \mathbf{d}\right), \quad (6)$$

$$\mathbf{p}_i = \mathbf{R}^T\left(\mathbf{P}_i - \mathbf{c}\right) , \quad (7)$$

where $\mathbf{R} \in SO(3)$ is the rotation matrix from the BB to the global coordinate systems, '$\times$' is the cross product operator and '$\circ$' is the element-wise product operator.

One of the main ideas behind these equations is the *action-counteraction requirement*. This requirement allows to prevent global displacements of the object by applying the half of the traction/compression inputs, from opposing directions at each of the two horizontal axes of the BB reference frame. The general rule for guaranteeing the action-counteraction requirement consists in positioning the N grippers around $\mathbf{c}$ so that they are separated less than π radians from each of the neighboring ones.

3.2 Model identification

Once the structure and properties of the model are set, a method for obtaining the 9 non-zero parameters of the Jacobian matrix $\mathbf{J}$, which depend on the object properties and the grasping configuration, is developed. The strategy consists in taking different measurements of $\dot{\mathbf{d}}$ and $\dot{\theta}_z$ from randomly chosen $\mathbf{u}$'s. Then, an estimate of the model parameters is obtained by solving the system of equations. An ordinary least-squares approach provides the solution by linearly adjusting the parameters to the set of $S > 3$ measurements:

$$\mathbf{J}_{vect} = [k_{11}, k_{12}, ..., k_{43}]^T = \left(\mathbf{A}^T\,\mathbf{A}\right)^{-1}\mathbf{A}^T\,\mathbf{b} , \quad (8)$$

$$\mathbf{A} = \mathrm{blkdiag}\Bigg(\begin{bmatrix} \dot{G}_{x1} & \dot{G}_{y1} \\ \dot{G}_{x2} & \dot{G}_{y2} \\ \cdots & \\ \dot{G}_{xS} & \dot{G}_{yS} \end{bmatrix}, \begin{bmatrix} \dot{G}_{x1} & \dot{G}_{y1} \\ \cdots & \\ \dot{G}_{xS} & \dot{G}_{yS} \end{bmatrix}, ..., \begin{bmatrix} \dot{G}_{x1} & \dot{G}_{y1} & \dot{\phi}_{z1} \\ \cdots & & \\ \dot{G}_{xS} & \dot{G}_{yS} & \dot{\phi}_{zS} \end{bmatrix}\Bigg) , \quad (9)$$

$$\mathbf{b} = \left[\dot{d}_{x1}, \dot{d}_{x2}, ..., \dot{d}_{xS}, \dot{d}_{y1}, ..., \dot{d}_{yS}, ..., \dot{\theta}_{zS}\right]^T . \quad (10)$$

The accuracy of the resulting model depends on the quality and the quantity of the S measurements. Instead of obtaining $\mathbf{J}$ from random $\mathbf{u}$'s, in both value and number, more robust estimates can be obtained by means of an *observability index*. The observability indexes, which derive from the *alphabet optimalities*, provide statistical information about the parameters variance and the numerical conditioning of the model by analyzing the numerical properties of the regressor matrix $\mathbf{A}$ [15]. Robot calibration techniques have exploited these indexes in multiple ways, either developing calibration techniques robust to sensor noise [16] or selecting the best index for different applications [17]. Therefore, selecting the inputs to the system as the ones that maximize one of these indexes is convenient not only to reduce the uncertainty of the parameters of $\mathbf{J}$, but also to decide the number of measurements to take. We study five different observability indexes and their utility for obtaining the DBB model, with $\sigma_L \leq \sigma_{L-1} \leq ... \leq \sigma_1$ the L singular values of $\mathbf{A}$: $O_1 = (\sigma_L\,\sigma_{L-1}\,...\,\sigma_1)^{1/L}/S^{1/2}$, $O_2 = \sigma_L/\sigma_1$, $O_3 = \sigma_L$, $O_4 = \sigma_L^2/\sigma_1$ and $O_5 = (\sum_{i=1}^{L} 1/\sigma_i)^{-1}$.

We optimize these indexes with a modified version of the DETMAX algorithm [18]. This algorithm improves the experiment design by iteratively exchanging inputs, so that an observability index is maximized for a fixed experiment size. The rows of $\mathbf{A}$ are inserted from a set of candidate inputs, which is created by combining different values of $\dot{G}_x$, $\dot{G}_y$ and $\dot{\phi}_z$ that lie within the expected operational limits. An optimal experiment design, and hence the regressor matrix $\mathbf{A}$, is obtained when the algorithm converges to a maximum index value. Then, the selected inputs are applied to the object to get the matrix of measurements $\mathbf{b}$ (see (10)). Finally, the model parameters are obtained from equation (8).

4. COLLISION AVOIDANCE WITH MINIMAL DISPLACEMENTS

As we stated previously, we propose to solve the problem of transporting a deformable object while avoiding collisions by means of optimization techniques. The current inputs $\mathbf{u}$ that will drive the object to the future

collision-free state are those that deform and rotate the DBB to avoid the incoming obstacles. Therefore, the optimization is not performed at the current position of the object and the manipulators, but it is applied to a BB with the centroid at the future position $\mathbf{c}'$. This future BB centroid is computed as the furthest point $\mathbf{r}_k$ lying within the detection range of the system and at a distance from the detection limit greater or equal than the semi-diagonal of the horizontal projection of the current BB. The vertical component is computed from the grippers' height.

We define the optimization problem at $\mathbf{c}'$ as follows:

$$\begin{aligned} &\text{Given} \quad \mathbf{P}, \mathbf{c}', \mathbf{d}, \mathbf{u}, \mathbf{J}, \mathbf{R} \\ &\underset{\mathbf{u}}{\text{minimize}} \quad \gamma \\ &\text{subject to} \quad \mathbf{C}, \mathbf{u}_{lim} \quad , \end{aligned} \tag{11}$$

where $\mathbf{C} = \{C_j,\, j = 1, ..., M\}$ is a set of nonlinear constraints, whose number coincides with the number of obstacle points, and $\mathbf{u}_{lim}$ includes the linear constraints with the upper and lower limits of $\mathbf{u}$.

The nonlinear constraints $\mathbf{C}$ are responsible of obstacle avoidance, and can be computed as:

$$C_j = \|\mathbf{B}_j\| - \|\mathbf{q}_j\| \leq 0 \,, \tag{12}$$

$$\mathbf{B}_j = -(\delta + \delta_s)(\mathbf{q}_j/\|\mathbf{q}_j\|)/(\mathbf{n}^T \cdot (\mathbf{q}_j/\|\mathbf{q}_j\|)) \,, \tag{13}$$

$$\mathbf{q}_j = \left(\mathbf{R} \begin{bmatrix} \cos(\theta'_z) & -\sin(\theta'_z) & 0 \\ \sin(\theta'_z) & \cos(\theta'_z) & 0 \\ 0 & 0 & 1 \end{bmatrix} \right)^T (\mathbf{Q}_i - \mathbf{c}') \,. \tag{14}$$

$\mathbf{B}_j$ is the intersection point between the ray $\mathbf{q}_j$, which is the obstacle point in the BB reference frame, and one of the box faces with normal $\mathbf{n}$ (column vectors $[1,0,0]^T$, $[-1,0,0]^T$, ..., $[0,0,-1]^T$). The scalar product $\mathbf{n}^T \cdot (\mathbf{q}_j/\|\mathbf{q}_j\|)$ indicates the relative orientation between the face normal $\mathbf{n}$ and $\mathbf{q}_j$. The intersections of $\mathbf{q}_j$ with the 6 faces of the BB are computed, and the one pointing towards the same side than $\mathbf{n}$ (positive scalar product), and being inside the face limits, is selected as the valid $\mathbf{B}_j$. The distance δ of a BB face to the origin, augmented by the safety threshold δ_s, and the face limits are computed from the estimated future state of the BB $[\mathbf{d}', \theta'_z]$. In turn, the future state of the BB is computed in the following manner:

$$[\mathbf{d}',\, \theta'_z]^T = [\mathbf{d},\, \theta_z]^T \circ (\mathbf{J}\ \mathbf{u}\ \Delta t) \,, \tag{15}$$

$$\Delta t = \|\mathbf{c}' - \mathbf{c}\| \,/\, \|\dot{\mathbf{P}}_t\| \,. \tag{16}$$

Then, if the inequality (12) holds $\forall j$, the nonlinear constraints are satisfied.

The linear constraints $\mathbf{u}_{lim}$ are obtained from the minimum and maximum dimensions ($d_w^{min}, d_w^{max}, w = \{x, y, z\}$) and rotations ($\theta_z^{min}, \theta_z^{max}$) of the BB:

$$\begin{bmatrix} (d_x^{max} - d_x)/d_x \\ (d_y^{max} - d_y)/d_y \\ (d_z^{max} - d_z)/d_z \\ \theta_z^{max} \end{bmatrix} \geq \mathbf{J}\,\mathbf{u}\,\Delta t \geq \begin{bmatrix} (d_x^{min} - d_x)/d_x \\ (d_y^{min} - d_y)/d_y \\ (d_z^{min} - d_z)/d_z \\ \theta_z^{min} \end{bmatrix} . \tag{17}$$

An optimal solution of this problem is provided by a *pattern search* optimization algorithm, which is able to handle the nonlinear constraints.

5. RESULTS AND DISCUSSION

We test the performance and validity of our DBB model and the optimization strategy by means of simulations in Matlab®. Different kinds of deformable objects and configurations are studied by modifying the properties of a mesh composed of standard mass–spring–damper elements.

5.1 Objects with different properties

The validity of our system is tested with materials of different mechanical properties. We define a base model consisting in a 2×3 meters mesh of mass–spring–damper elements (see Fig. 1), with 150 nodes and stiffness, damping and nodal mass of 20 N/m, 0.5 N s/m and 0.01 kg respectively. Note that the model properties are completely unknown to the system. A set of 20 different objects is created by evenly increasing the stiffness of the base model from 20 to 970 N/m, while the damping, nodal mass and number of nodes are left unaltered to avoid combined effects (for instance, increasing the nodal mass at the same time as stiffness could compensate vertical deformations). The objects are held by four grippers, one at each corner, and the DBB model is obtained by maximizing O_1 from a set of $S = 8$ measurements. We consider O_1 because this observability index provides the most accurate DBB models, in terms of mean squared error, and the amount of 8 measurements due to a convenient balance between model accuracy and computational cost. After this, the object is transported following a specified linear trajectory across a circuit, which contains a narrow corridor (2.5 m wide and 1920 points) and a short cylinder (1.0 m in height and 180 points) as obstacles (see Fig. 2). The perception range R is set to 5.0 m, and a value of $\delta_s = 0.3$ m is chosen for guaranteeing collision avoidance in all cases.

After running the simulations for all the proposed materials, the values of several variables have been collected. Figure 3 shows, at the top, two box plots with the cost function values γ of the tested materials, at those simulation instants where obstacles are detected and the optimization is executed. In the top plot we have aggregated the values γ of all materials, and the bottom plot includes the mean values of γ in each simulation. We can see that the mean values for all materials are quite similar, and no outliers appear in the upper box plot. The lower box plot shows that the objects with lower stiffness, 20 N/m and 70 N/m, show higher γ values. This is due to the fact that higher deformations are required to compensate the greater flexibility of these objects. Figure 4 includes, at the top, the box plots of 45 different simulation instants. The box plots represent the aggregated distances of each node in the object meshes of all materials to their nearest obstacle point. In case the node is contained in the convex hull of an obstacle, i.e. if collision occurs, the distance is negative. Therefore, collision avoidance is verified by the fact that all distances in the plots are greater than zero. Considering these results, and the fact that all models are linear elastic and the geometric

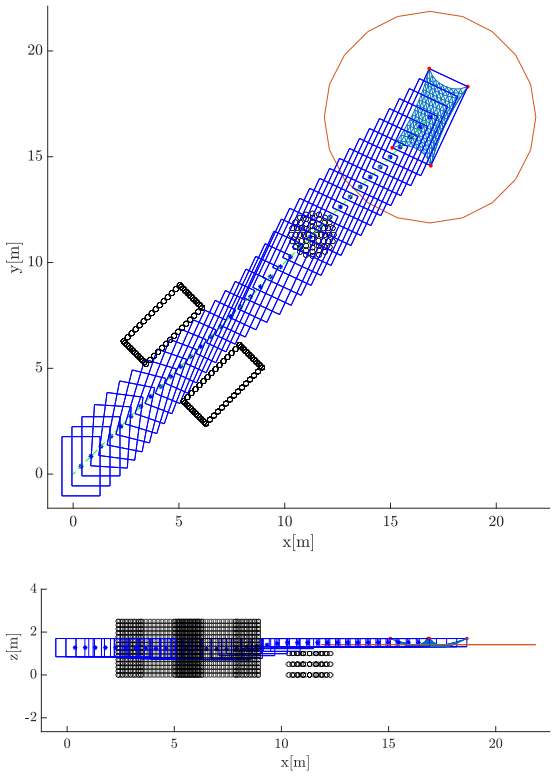

Fig. 2. First test circuit (top view and side view below). Starting at (0,0,1.7) and following the linear trajectory in green, the object is transported by 4 grippers represented with red dots. The deformable object is depicted as a blue mesh, with an orange circumference around it that represents the perception range of the system. The obstacles, in black, are a narrow corridor in the left corner of the image and a short cylinder in the middle. The BBs of the object over time are represented as blue boxes.

nature of our system, it can be seen that the performance of the model is not significantly affected by the variations in the object mechanical properties. The average computational cost of an optimization is 0.4525 seconds with a 3.20 GHz Intel Core i7-8700 CPU.

5.2 Number and position of the grippers

The configuration of grippers transporting the object also affects the DBB model. In this section, we analyze this influence with 8 different gripper configurations. These configurations are created with an increasing number of grippers $N = 3, ..., 10$, which are positioned around the object's boundary with the angular rule $2\pi i/N$. Folds and wrinkles are created in the object with this configuration rule, which allows us to test this kind of effects in the system. The mechanical properties of the object are the ones of the base model, but the stiffness is modified to 400 N/m. The perception range R is again set to 5.0 m, and a value of $\delta_s = 0.25$ m is chosen.

In the circuit for these tests (see Fig. 5), the object follows a 10 m radius semicircular trajectory that goes over a pair of short cylinders (0.7 m in height and 174 points) and next to a wall (1.5 m wide, 1368 points). We

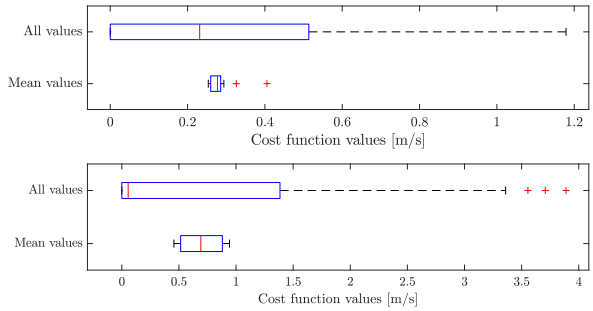

Fig. 3. Box plots with all γ values and the mean value of γ in each simulation. At the top, we show the results with the 20 different materials, and at the bottom the results with the 8 different gripper configurations.

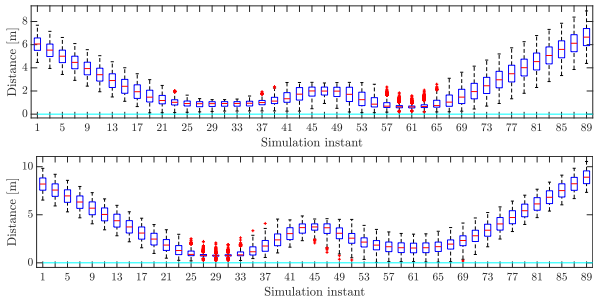

Fig. 4. Box plots of the distances of each node in the object mesh to the nearest obstacle, at 45 simulation instants. The top box plots contain the distances from the meshes with all the considered materials. The bottom box plots contain the distances from the meshes with the 8 different gripper configurations. We can see that no collisions occur since all distances are greater than zero, which means that the mesh nodes are outside of the convex hull of the obstacles.

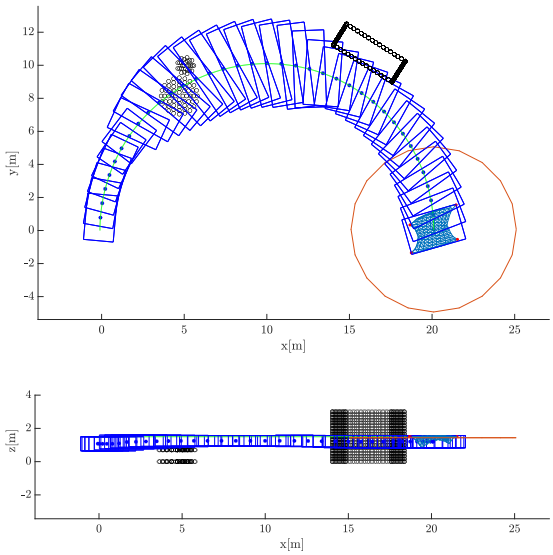

Fig. 5. Second test circuit (top view and side view below). In this case, 4 grippers transport the object following a 10 m radius semicircular trajectory (in green) that goes over the cylinders and next to the wall.

compare again the values of γ for the different configurations at those simulation instants where the optimization is executed in Fig. 3, at the bottom. As in the previous tests, the highest cost values correspond to the cases with the most flexible objects, i.e. when the mesh is held by 3 and 4 grippers. The box plots over time with the distances from the mesh nodes to the nearest obstacle point, in all configurations, are depicted in Fig. 4 at the bottom. It can be seen that collisions are prevented in all cases when the objects go over the cylinders as well as next to the wall, with minimal distances greater than zero at every simulation instant. The average computational cost of an optimization execution is 0.2931 s. To summarize, we have verified that the DBB model and the optimization strategy are valid for different gripper configurations with no significative affection to its performance even in the presence of folds and wrinkles.

6. CONCLUSION

We have presented a novel method for multi-robot transport of deformable objects with collision avoidance. The core of the method is a new model based on the paradigm of *deformable bounding box*. This model can be obtained with a small number of measurements thanks to the maximization of the observability index O_1. Once obtained, it is introduced into an optimization loop that minimizes the grippers velocities at the same time that obstacles are avoided. We have reported simulation results that show the validity and performance of our system in different scenarios and with different system configurations. We think this strategy has potential applications that may be useful for different purposes, thanks to its adaptability to general transport problems.

REFERENCES

[1] J. Sanchez, J. A. Corrales, B. C. Bouzgarrou, and Y. Mezouar, "Robotic manipulation and sensing of deformable objects in domestic and industrial applications: a survey," *Int. J. Robotics Research*, vol. 37, no. 7, pp. 688–716, 2018.

[2] Z. Feng, G. Hu, Y. Sun, and J. Soon, "An overview of collaborative robotic manipulation in multi-robot systems," *Annual Reviews in Control*, vol. 49, pp. 113–127, 2020.

[3] R. Herguedas, G. Lopez-Nicolas, R. Aragues, and C. Sagues, "Survey on multi-robot manipulation of deformable objects," in *IEEE ETFA*, 2019, pp. 977–984.

[4] M. Ruan, D. McConachie, and D. Berenson, "Accounting for Directional Rigidity and Constraints in Control for Manipulation of Deformable Objects without Physical Simulation," in *IEEE/RSJ IROS*, oct 2018, pp. 512–519.

[5] K. Hosoda and M. Asada, "Versatile Visual Servoing without Knowledge of True Jacobian," in *IEEE/RSJ IROS*, 1994, pp. 186–193.

[6] D. Navarro-Alarcon, Y. H. Liu, J. G. Romero, and P. Li, "Model-free Visually Servoed Deformation Control of Elastic Objects by Robot Manipulators," *IEEE Transactions on Robotics*, vol. 29, no. 6, pp. 1457–1468, 2013.

[7] S. Jin, C. Wang, and M. Tomizuka, "Robust Deformation Model Approximation for Robotic Cable Manipulation," in *IEEE/RSJ IROS*, nov 2019, pp. 6586–6593.

[8] O. Burchan Bayazit, J.-M. Lien, and N. M. Amato, "Probabilistic Roadmap Motion Planning for Deformable Objects," in *IEEE ICRA*, 2002, pp. 2126–2133.

[9] R. Buchanan, T. Bandyopadhyay, M. Bjelonic, L. Wellhausen, M. Hutter, and N. Kottege, "Walking Posture Adaptation for Legged Robot Navigation in Confined Spaces," *IEEE RA-L*, vol. 4, no. 2, pp. 2148–2155, 2019.

[10] R. Tallamraju, D. H. Salunkhe, S. Rajappa, A. Ahmad, K. Karlapalem, and S. V. Shah, "Motion Planning for Multi-Mobile-Manipulator Payload Transport Systems," in *IEEE CASE*, 2019, pp. 1469–1474.

[11] H. G. Tanner, S. G. Loizou, and K. J. Kyriakopoulos, "Nonholonomic Navigation and Control of Cooperating Mobile Manipulators," *IEEE Transactions on Robotics and Automation*, vol. 19, no. 1, pp. 53–64, 2003.

[12] J. Alonso-Mora, R. Knepper, R. Siegwart, and D. Rus, "Local motion planning for collaborative multi-robot manipulation of deformable objects," in *IEEE ICRA*, 2015, pp. 5495–5502.

[13] K. Hunte and J. Yi, "Collaborative Object Manipulation Through Indirect Control of a Deformable Sheet by a Mobile Robotic Team," in *IEEE CASE*, 2019, pp. 1463–1468.

[14] G. Lopez-Nicolas, R. Herguedas, M. Aranda, and Y. Mezouar, "Simultaneous shape control and transport with multiple robots," in *IEEE International Conference on Robotic Computing (IRC)*, 2020, pp. 218–225.

[15] J. Hollerbach, W. Khalil, and M. Gautier, "Model Identification," in *Springer Handbook of Robotics*, 1st ed., B. Siciliano and O. Khatib, Eds. Springer Berlin Heidelberg, 2008, ch. 14, pp. 321–344.

[16] D. Daney, Y. Papegay, and B. Madeline, "Choosing Measurement Poses for Robot Calibration with the Local Convergence Method and Tabu Search," *Int. J. Robotics Research*, vol. 24, no. 6, pp. 501–518, 2005.

[17] A. Joubair, A. Tahan, and I. Bonev, "Performances of observability indices for industrial robot calibration," in *IEEE/RSJ IROS*, 2016, pp. 2477–2484.

[18] T. J. Mitchell, "An Algorithm for the Construction of "D-Optimal" Experimental Designs," *Technometrics*, vol. 16, no. 2, pp. 203–210, 1974.